Applied Physics A (2020)126:923
https://doi.org/10.1007/s00339-020-04100-5

Applied Physics A
Materials Science & Processing

Charge carrier performance of phosphazene-based ionic liquids doped hole transport layer in organic light-emitting diodes

Selin Pıravadılı Mucur[1] · Betül Canımkurbey[2,3] · Pelin Kavak[4] · Hüseyin Akbaş[5] · Ahmet Karadağ[6]

Received: 19 July 2020 / Accepted: 21 October 2020
© Springer-Verlag GmbH Germany, part of Springer Nature 2020

Abstract

The enhancement of hole injection layers is strongly important issue for obtaining high-efficient and low-driving-voltage Organic Light-Emitting Devices (OLEDs). In this paper, we presented a comprehensive electroluminescence (EL) study of phosphazene-based ionic liquids (PzILs) used as a hole transport layer in solution-processed OLEDs. Charge transfer properties of PzILs were investigated by doping in poly(3,4-ethylenedioxythiophene) polystyrene sulfonate (PEDOT:PSS) at different ratios (0.1, 0.2, 0.5, 1.0, 2.0). Previously synthesized four types of PzILs (namely PzIL1, PzIL2, PzIL3, and PzIL4) were prepared in de-ionized water with 10 mg/ml concentration, mixed with PEDOT:PSS and examined for their charge transport characteristics on OLED device performance due to their ionic nature. The device with PzIL1 exhibited the best performance with luminance 4185 cd/m^2 compared to other devices with and without PzILs. Further, Density Functional Theory (DFT) calculations and admittance spectroscopic analysis of OLEDs based on four types of PzILs were studied profoundly. Admittance spectroscopy has been used for revealing the carrier transport properties, mobility and the equivalent circuit modeling of the devices. Four types of PzILs OLEDs represented typical p-type transporting characteristics with moderate mobility up to 1.93 cm^2/V.s.

Keywords Organic light-emitting diodes (OLEDs) · Phosphazene-based ionic liquids · PEDOT:PSS · Charge transfer · Admittance spectroscopic analysis

1 Introduction

OLEDs take part in next-generation display markets due to their energy saving, high efficiency, environmental friendliness, flexibility and easy fabrication features [1–5]. Especially, solution-processed OLEDs are widely searched and studied because of their cheaper, easier and time-saving fabrication [6–10]. The power consumption of OLEDs is one of the most crucial issues for commercial applications up to date. The low energy barrier is required at the interface between the layers for efficient charge injection and low power consumption. Therefore, the main goal is to achieve high-efficiency solution-processed OLEDs with low-driving voltages, so that, the development of charge transport materials becomes necessary for the device working principle [11, 12]. The hole injection ability of the hole transport and injection layers (HTLs and HILs, respectively), such as poly(3,4-ethylenedioxy-thiophene):poly(styrene sulfonate) (PEDOT:PSS) [13, 14] and polyaniline, etc., of thin films are determinants for the anode part performance of solution-processed OLEDs [15–17]. The easy deposition processing

✉ Betül Canımkurbey
betul.canimkurbey@amasya.edu.tr;
bcanimkurbey@gmail.com

1 Materials Institute, The Scientific and Technological Research Council of Turkey (TUBITAK), Marmara Research Center (MAM), 41470 Gebze, Kocaeli, Turkey

2 S. Şerefeddin Health Services Vocational School, Amasya University, 05100 Amasya, Turkey

3 Central Research Laboratory, Amasya University, 05100 Amasya, Turkey

4 Physics Department, Yıldız Technical University, Esenler, 34220 Istanbul, Turkey

5 Department of Chemistry, Tokat Gaziosmanpaşa University, 60250 Tokat, Turkey

6 Department of Chemistry, Yozgat Bozok University, 66200 Yozgat, Turkey

Published online: 06 November 2020

by spin-casting technique from solution makes PEDOT:PSS favorable among the HILs. It has become commercially most popular and successful conductive polymer with its stability, fine electrical and optical properties which are important for optoelectronic device technology. PEDOT: PSS deposited between ITO and emissive layer provides electrical anode contact so that a notable rise in the lifetime of OLEDs could be obtained, because PEDOT:PSS preserves emissive layer from the migration of oxygen-involving species in ITO contact and balancing the energy difference between ITO and emissive polymer [18]. The thin films with PEDOT:PSS have less than 5.0 nm a surface roughness and good photo and electrical stability in the air. PEDOT:PSS conductivity can be enhanced twice times due to the inclusion of alcohol and its additives (ethylene glycol, mesoerythritol, 2-nitroethanol, sorbitol) or DMF and DMSO [19–23]. From this point on, we doped PEDOT:PSS with ionic liquid (IL) with different concentration to observe the effect of ILs on device characteristics. In this study, previously synthesized PzILs used in HIL in solution-processed OLEDs [24, 25]. ILs are salts that are in liquid form at room temperatures, with relatively weak coulombic interactions between cations and anions [26–28]. Cyclophosphazenes containing phosphorus–nitrogen double bond in their skeletons are more stable than other phosphazene compounds and are, therefore, the best known and most intensively studied phosphazene compounds [29]. There are many applications related to cyclophosphazenes, such as biomedical materials [30], liquid crystals [31], lubricants [32], electrical conductors [33], Li-ion batteries [34], and OLEDs [35, 36]. PEDOT: PSS is known to exhibit degradation problems in some applications, such as hall transport layers in OLED due to the acidity and water availability of PSS. Therefore, hydrophobic PEDOT/IL dispersions are studied as alternative hall injection materials for OLED applications [37–40]. Henk J. Bolink et al. introduced a new approach for fabricating efficient hybrid organic–inorganic inverted light-emitting diodes by adding additives to metal oxide solutions to use in interfacing layers. For this purpose, the precursor solution of ZnO was mixed with IL to obtain doped-ZnO. Thus, ZnO: ILs cathode was attained that ascended the electron injection properties [41]. S. Ohisa et al. used IL-based electron injection layers (EILs) for solution-processed OLEDs. Device showed lower-driving voltages than conventional OLED devices containing an alkali–metal complex (8-quinolinolato lithium) as EIL. The longer alkyl chain of ILs in EIL was considered to be more effective in decreasing driving voltage [42].

In addition to these studies, T.Y. Kim et al. studied the lifetime of OLEDs with PEDOT:IL to get polymeric hole-injecting material capable of improving device lifetime. They concentrated on the lifetime of the OLED by comparing PEDOT:PIL and PEDOT:PSS. The devices based on PEDOT:IL showed a significantly longer lifetime, which was attributed to the effective protection characteristic of PEDOT:IL for indium extraction from ITO electrode. Although the enhancement on the current efficiency and luminance was small, the lifetime of the OLED with PIL was significantly enhanced [39].

In our contribution, the enhancement effect of the PzIL1-4 on the polymer OLED characteristics was systematically investigated. PzIL1-4 was applied to an OLED structure and characterized for the first time. In the fabrication of the OLEDs, different ratios (1:0.1, 1:0.2, 1:0.5, 1:1, 1:2) of PEDOT:PSS:PzIL1-4 blends were used as a HIL, poly[2-methoxy-5-(2-ethylhexyloxy)-1,4-phenylene vinylene] (MEHPPV) was used as an emissive layer and calcium (Ca)/aluminum (Al) were cathode side of the device. Chemical structure of four types of PzILs could be seen from Fig. 1, namely PzIL1, PzIL2, PzIL3 and PzIL4. For the comparison of the performances, the reference device without PzILs was also fabricated. They were prepared in de-ionized water with 10 mg/ml concentration, mixed with PEDOT:PSS and examined for their charge transport characteristics on OLED device performance due to their ionic nature. Impacts of the PzILs on device performances, such as onset voltage, luminance, current efficiency and EL intensity of the devices, were investigated. Thus, PzIL1-4-based HILs were expected to generate large electric field-induced polarization, which would result in low-driving voltage devices than the device without PzILs, because of the high mobility of the ions of ILs due to polarization generated by the large electric field. PzIL1 with trimethylammonium-ethoxy and PzIL2-4 with trimethylammonium-propoxy chains whose anions were iodide have different cationic parts (Fig. 2). The effect of these differences (side alkyl chain length and spiro ring) on OLED characteristics was also investigated. The side-chain length of PzIL1 was shorter than the others. PzIL2 consisted of a six-membered spirocyclic ring, while the other PzILs (PzIL1, PzIL3 and PzIL4) consisted of a five-membered spirocyclic ring. Among these PzILs carrying secondary amino and pendant (4-fluorobenzyl)spiro groups, PzIL4 contained a terminal ethyl group, while PzIL1-3 contained a terminal methyl group. The PzIL-based OLEDs exhibited reducing driving voltages than the reference device (without PzILs) that coherent with the literature.

Further, the device with PzIL1 exhibited the best performance with luminance 4185 cd m^{-2} compared to other devices with and without PzILs. It had a current efficiency of 0.49 cd A^{-1} and external quantum efficiency (EQE) 0.24%. DFT calculations and admittance spectroscopic analysis of OLEDs based on four types of PzILs were worked through comprehensively. Admittance spectroscopy has been used for revealing the carrier transport properties, mobility and the equivalent circuit modeling of the devices. PzIL1-4-based OLEDs represented typical p-type transporting characteristics with maximum mobility 1.93 cm^2/V.s.

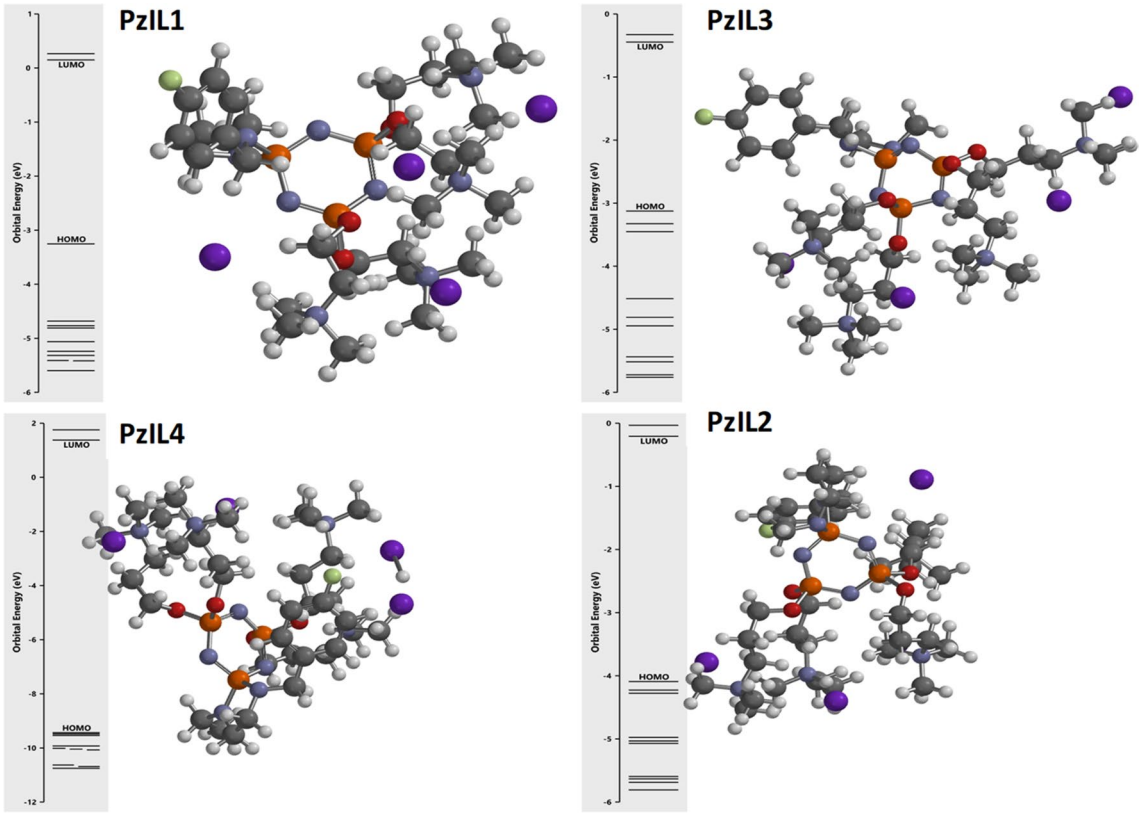
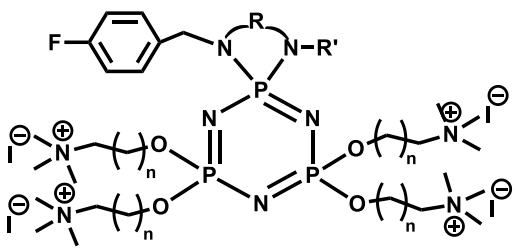


Fig. 1 Chemical structure of PzIL1-4

Fig. 2 General structure of PzIL1-4



	R	R'	n
PzIL1	$(CH_2)_2$	CH_3	1
PzIL2	$(CH_2)_3$	CH_3	2
PzIL3	$(CH_2)_2$	CH_3	2
PzIL4	$(CH_2)_2$	CH_2CH_3	2

2 Experimental

The Plasma Etch system was utilized for cleaning the ITO-coated substrates. PEDOT:PSS was supplied from Heraeus Clevios GmbH. Before the fabrication of OLEDs, patterned ITO-coated glass substrates (Kintec Company) were cleaned ultrasonically in acetone, de-ionized water and alcohol in an ultrasonic bath. Afterwards, substrates were cleaned via oxygen plasma (Plasma Etch) treatments.

Hamamatsu PMA-12 C10027 Photonic Multichannel analyzer and digital multimeter (2427-C 3A Keithley) were used to measure EL, luminance, EQE, current efficiency, the current density–voltage relation of the devices with various PzILs ratios. KLA Tencor P-6 stylus profiler was used to measure thickness of thin films and the PzILs thin films were scanned with atomic force microscopy (Park Systems XE150) were used to determine the roughness with the 3 μm × 3 μm measurement area. SOIF Inst. optical microscope was utilized to investigate the film surfaces. PEDOT: PSS was spin-coated onto the pre-cleaned ITO-coated glass at 3000 rpm for 60 s and then cured at 120 °C for 15 min. MEHPPV was prepared by dissolving in a toluene concentration of 8.0 mg/ml and deposited on top of the HIL by spin-coating at 1500 rpm for 60 s then baked at 60 °C under its T_g for 10 min in N_2 environment. Finally, Ca as an EIL and a cathode layer of Al were deposited by thermal evaporation under 1×10^{-6} mbar. The emission area is 9.0 mm^2. The devices with ITO/PEDOT:PSS with PzIL1-4/MEHPPV/Ca/Al structure were fabricated.

Interdigitated gold electrodes fabricated on glass substrate by lithography process were used for dielectric measurements. These electrodes were shown in Fig. 3, have 100 µm channel width. Then, PzIL1-4 was dropped cast on interdigitated electrodes.

2.1 Theoretical study

The optimized geometry and the electron density distribution of the frontier molecular orbitals (FMOs) were investigated using DFT (Spartan 18 software, Wavefunction [43]) calculations with the B3LYP (Becke 3-parameter-Lee Yang-Parre) with the basis set of 6-311G (d,p). PzIL1-4 was fully geometry optimized at the B3LYP level using the corresponding PM6 equilibrium geometry structures as input. In Fig. 4, it was seen that calculated molecular orbitals (The highest occupied molecular orbital (HOMO) and lowest unoccupied molecular orbital (LUMO)) energies (E_{HOMO} and E_{LUMO}) for PzIL1-4 with B3LYP/6-31G(d,p) level. These theoretical calculations were important to investigate the location of carriers on the PzIL1-4, therefore, it helped to comment for the device working principle. As expected, the energy value of PzIL2, which had a six-membered spiro ring, was found to be the highest value (Table 1).

The energy levels of the molecular orbitals HOMO and LUMO for PzIL1-4 informed about the possible electronic transition and indicated the electrophilic and nucleophilic attraction in the ILs. The LUMO-HOMO gap was also a significant parameter for the chemical reactivity.

The type and number of functional groups can have a significant effect on the HOMO-LUMO gap of the molecule. It can be said that there is the greatest increase in the HOMO-LUMO gap in PzIL4 compound containing oxygenated functional groups and a terminal ethyl group in the spiro ring. When PzIL2 and PzIL3 compounds with only different spiro rings were compared, it was seen that the HOMO-LUMO gap was higher in PzIL2 with more –CH 2 group.

PzIL4 had the biggest gap with 10.81 eV; therefore, it had the lowest reactivity. The shorter LUMO-HUMO gap is considered as the high reactivity. These values also gave information about the ionization potential according to Koopmans' theorem (IP = Negative of the HOMO energy) and electron affinity (EA = Negative of the LUMO energy).

$$IP = -E_{HOMO} \quad (1)$$

$$EA = -E_{LUMO} \quad (2)$$

When investigating the Table 1, PzIL4 had the highest IP which meant that the amount of energy required to remove one electron from PzIL4 atoms was the highest. This could be commented with higher LUMO energies of the PzIL1-4 leading to more stable ILs. Therefore, from Table 1, it could be concluded from EA values that the order in resistance against reduction is PzIL4 > PzIL1 = PzIL3 ~ PzIL2.

ILs consisting of cations with longer alkyl side chains were more stable with respect to reduction. PzIL4 contained a terminal ethyl group (CH_2CH_3). This was consistent with experimental observations [44] but the longer alkyl side chains led to a lower conductivity. This might be the distinctive cause of the lower mobility of PzIL4. Therefore, it was not applicable to increase the length of the alkyl chain to obtain high current efficiency for OLED devices. This was also coherent with J–V curves of the OLED devices. PzIL1 showed higher conductivity than the other at the same voltage.

From Fig. 4, it can be concluded that the LUMO of PzILs was totally located on the phosphazenium cationic side, and HOMO of PzILs was located on the iodide anionic side. Since the LUMO was located completely on the cation, the resistance of the cation against reduction determined the stability with respect to the reduction of the IL predominantly. This gave us information about the hardness and softness properties of the ionic molecules. The hardness of an ion or molecule is a qualitative indication of polarizability in an electric field. The hardness and softness which are the reciprocal of the hardness, were mentioned suggested in literature [45] to describe resistance to deformation by external force. The hardness (η) and softness (σ) of a chosen molecule calculates the energy gap between the HOMO and LUMO orbitals and can be expressed as:

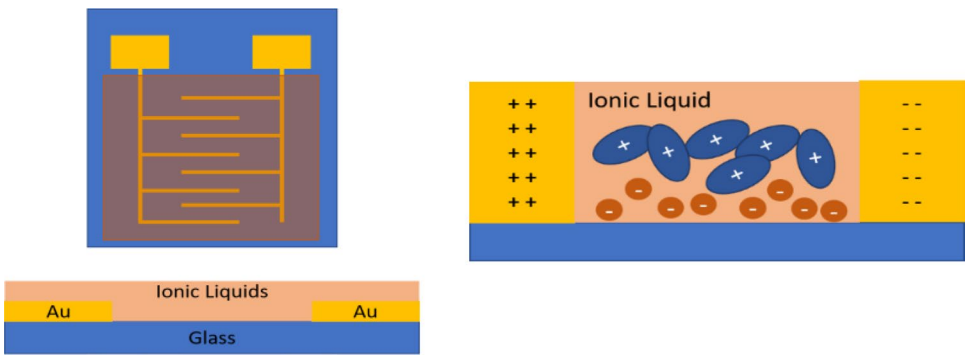


Fig. 3 Schematic structure of fabricated capacitors with PzIL 1-4 for impedance spectroscopy

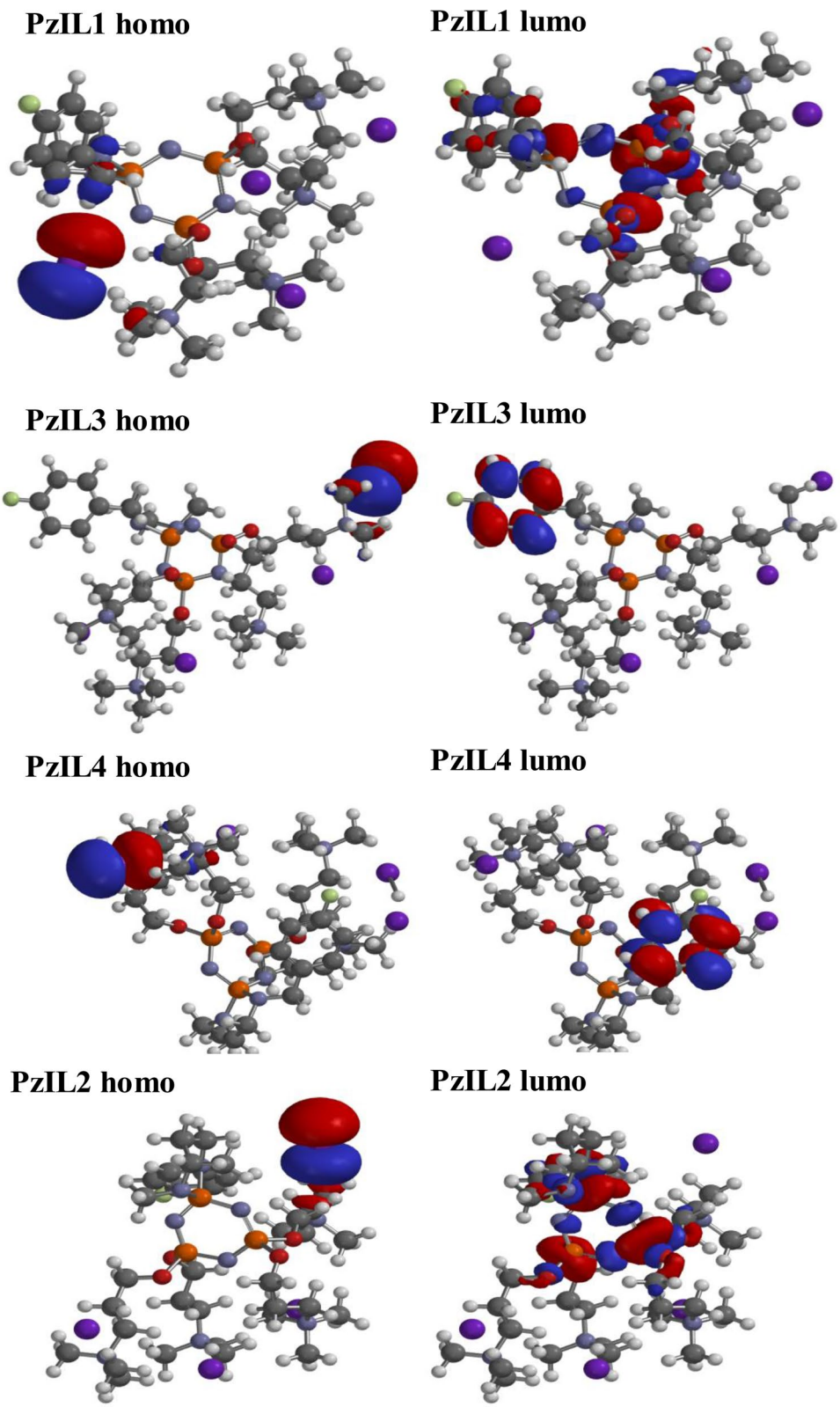


Fig. 4 Calculated molecular orbitals (HOMO and LUMO) energies (E_{HOMO} and E_{LUMO}) for PzIL 1-4 with B3LYP/6-31G(d,p) level

Table 1 DFT Calculations of FMOs of PzIL1-4

Ionic Liquids	HOMO (eV)	LUMO (eV)	Energy (au)	Band gap (eV)	IP (eV)	EA (eV)
PzIL1	− 3.25	0.15	− 3145.2	3.40	3.25	− 0.15
PzIL2	− 4.09	− 0.21	− 3342.0	3.88	4.09	0.21
PzIL3	− 3.13	0.15	− 3202.5	3.28	3.13	− 0.15
PzIL4	− 9.43	1.38	− 3325.1	10.81	9.43	− 1.38

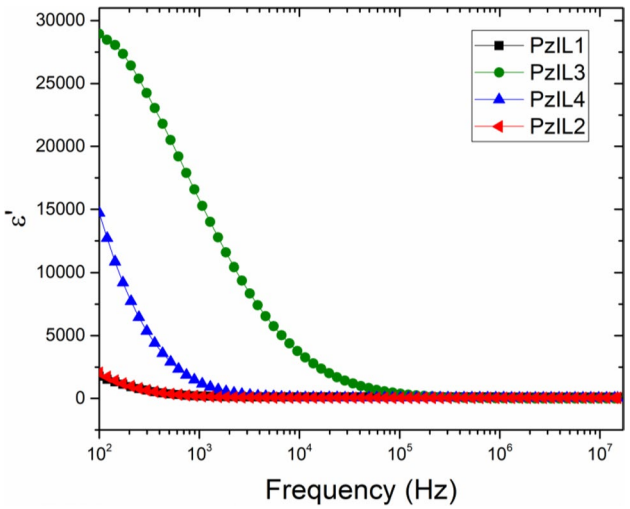


Fig. 5 PzIL1-4-coded real dielectric constant of the ILs change according to frequency

$$\eta = E_{LUMO} - E_{HOMO} \tag{3}$$

$$\sigma = \frac{2}{E_{LUMO} - E_{HOMO}} \tag{4}$$

Molecules with large HOMO-LUMO gap possess higher stability and opposing charge transfer. Molecules which have a small energy gap for its excitation are known soft molecules, which means easy in being polarizable. Therefore, for the chemical change property, soft molecules are more reactive than hard molecules. In this study, hardness arrangement was PzIL4 > PzIL2 ~ PzIL1 ~ PzIL3. PzIL4 showed highest resistance to polarization and the others PzIL1-3 showed nearly the same resistance to polarization.

2.2 Dielectric measurements

The dielectric measurements of the synthesized PzIL1-4 were performed at 100 Hz–15 MHz frequency. Frequency changes of real dielectric constants of the PzIL1-4 were given in Fig. 5. Figure 5 showed the change of the real dielectric constant of PzIL1-4 according to frequency. As it can be seen, the real dielectric constant of PzIL3 was larger than PzIL1, PzIL4 and PzIL2.

Therefore, the polarization was greater in these IL samples. The frequency variation trends of all three samples were approximately similar. Low-frequency permittivity of PzIL3 was very high [46], which was caused by diffusion of ions near the ITO–HIL interface. For PzIL3, ε_r' decreased strongly up to approximately 10 kHz, then this deceleration slowed down. The increase in frequency and this decrease in ε_r' were associated with the electrical relaxation process. But at the same time, there was a strong electrode polarization, as the electrolytic double layer was formed on the electrodes because of being IL. At higher frequencies, the molecules started to move slowly because they no longer followed the applied electric field. Consequently, energy consumption decreased and the decrease in ε_r at high frequencies slowed down. The real dielectric constants of the frequency domain outside of the electrode polarization were fitted with the Cole–Cole equation given in Fig. 6 for all samples. Figure 6 insets showed an electrical equivalent circuit model used for PzIL1-4. The Cole–Cole equation conformed to the symmetrically distributed polarization processes.

In this frequency region, the dielectric constant might contribute to ionic and orientation polarization. Dielectric parameters obtained for all PzIL1-4 were given in Table 2.

$$\varepsilon'(\omega) = \varepsilon_\infty + (\varepsilon_s - \varepsilon_\infty)\frac{1 + (\omega\tau)^{1-\alpha}\sin\left(\frac{1}{2}\alpha\pi\right)}{1 + 2(\omega\tau)^{1-\alpha}\sin\left(\frac{1}{2}\alpha\pi\right) + (\omega\tau)^{2(1-\alpha)}} \tag{5}$$

Here, ε_s was the static dielectric constant of the material before relaxation time and ε_∞ was the dielectric constant at the high-frequency limit after the relaxation time. $\omega = 2\pi f$, angular frequency, τ was the relaxation time. α was a constant related to the loss of a sample ranging from 0 to 1. It was related to the distribution of relaxation time, and if $\alpha = 0$, it was seen Debye relaxation time with a single relaxation time. The mobilities of devices with PzIL1-4 have been calculated using following formula where ϵ_0 was vacuum permittivity (8.85×10^{-2} F/m), ϵ relative material permittivity, i current, μ charge carrier mobility [5]. Calculated mobility data were also given in Table 2.

$$\mu = \frac{d^2}{iR^2C}\frac{1}{\left(1 + \sqrt{\frac{dC}{\varepsilon\varepsilon_0}}\right)}\sqrt{\frac{dC}{\varepsilon\varepsilon_0}} \tag{6}$$

Ions were restricted by the large coulombic interactions between cations and anions, ionic compound is difficult to form using large electric polarization. The reason for the weakening of the attractive interaction between cations and anions in ILs was the delocalization of the positive charge towards the p-conjugated part and the steric barrier of the alkyl chain.

The spectral response of ε was consistent with the relaxation behavior of ILs in the literature [47].

The mobility of PzIL1 with 1.93 cm^2/V.s was the best value when compared to other PzILs. PzIL3-4 with a longer terminal ethyl group showed the lowest mobility values. When the mobility of PzIL1-3 with the same terminal methyl group was compared, the mobility value of PzIL1 with the shortest side alkyl chain length was the highest. This value was higher than the mobility of the transistors fabricated with IL in the literature [48]. As a result, it was found that the mobility value decreased with increasing alkyl chain length [49].

2.3 Electroluminescence properties

Fabricated PzIL1-4 containing OLED device structure could be seen from Fig. 7a. The production procedure was discussed in detail in the experimental section. As the intention was the enhancement the HIL performance, MEHPPV commercial polymer was used as an emissive layer due to its known performance and optimized fabrication process

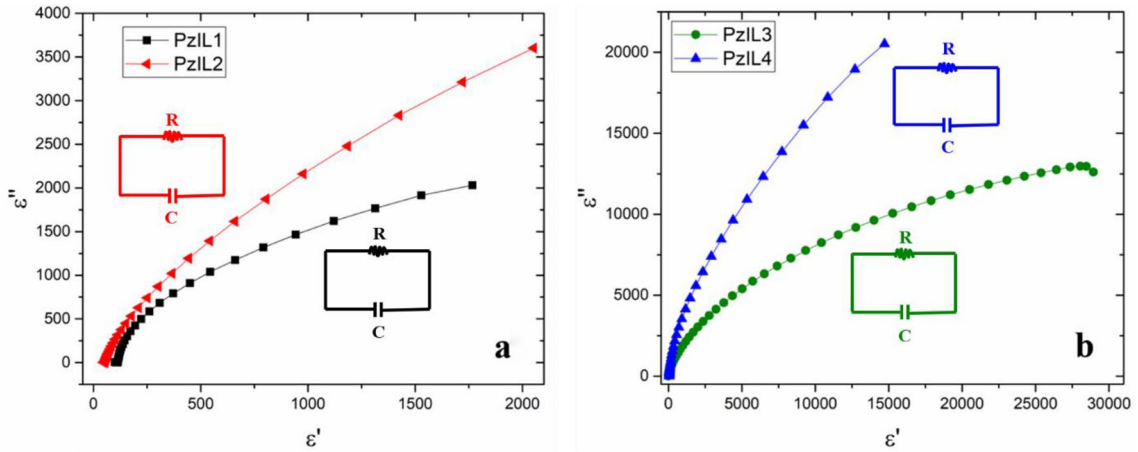


Fig. 6 **a** PzIL1- and PzIL2-, **b** PzIL3- and PzIL4-coded Cole–Cole plots of the ILs. The insets show electrical equivalent circuit model used for ILs

Table 2 Dielectric parameters for the PzIL1-4

Ionic Liquids	ε_s	ε_∞	τ (s)	α	σ_0 (S/cm)	μ (cm^2/V.s)
PzIL1	26.5 ± 0.7	5.44 ± 0.17	3.6E-7 ± 3.2E-8	0.46 ± 0.02	6.2E-6 ± 3.2E-8	1.93
PzIL2	37.5 ± 0.8	4.7 ± 0.1	2.2E-6 ± 1.7E-7	0.49 ± 0.008	4.2E-6 ± 1.7E-8	1.78
PzIL3	8.70 ± 0.7	3.29 ± 0.02	2.5E-6 ± 8.8E-7	0.45 ± 0.02	2.7E-8 ± 1.6E-10	0.025
PzIL4	49.8 ± 0.4	5.8 ± 0.1	2.6E-6 ± 7.3E-8	0.46 ± 0.003	3.0E-6 ± 1.9E-8	0.073

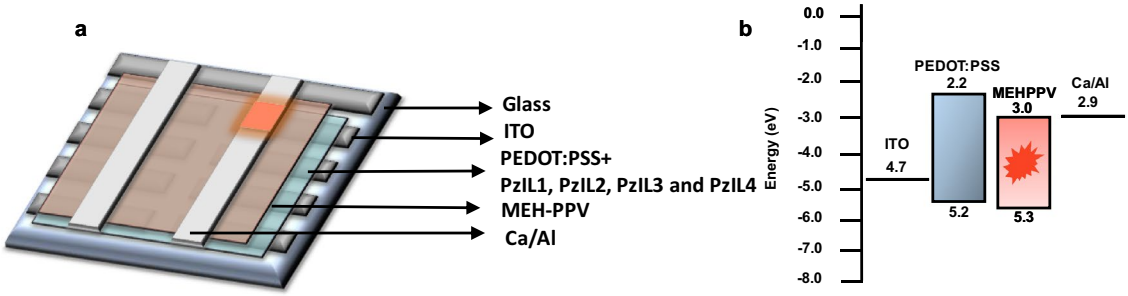


Fig. 7 **a** Schematic structure of OLED fabricated in this study, **b** energy diagram OLED; HOMO and LUMO band energies

in our earlier studies [50]. In this study, the key parameter was to find out the effect of PzILs in HIL on the device performance. It was clearly seen from Fig. 7b that the HOMO energy level of MEHPPV polymer and PEDOT: PSS was matched for injecting holes easier from ITO to the emissive layer. The LUMO energy level (− 3.0 eV) of MEHPPV was suitable for the transmission of electrons from the cathode.

Accomplished device characteristics for PzIL1-4, namely voltage–current density, EQE, light output, current efficiency and EL spectra, were determined and carefully analyzed to clarify the impacts of PzILs on the device carrier physics phenomena. Electric field-induced polarization was caused by the movements of ions in ionic compounds, therefore, the enhancement of the performances was observed in this part. On the other hand, EL spectra were not significantly affected (± 10 nm) by embedding PzIL1-4 to HILs of OLEDs. This meant the performance increase could only be interpreted by the increase in the movement of the charge carriers due to polarization, resulting in more efficient combination in the emission layer. Here, current efficiency is the luminous intensity per ampere and EQE in OLED is defined as the ratio of extracted photons over injected charges. In this study, device 0.1, 0.2, 0.5, 1.0 and 2.0 PzILs signified that the amount of PzILs (in ml) was mixed in 1.0 ml PEDOT:PSS.

Various ratios of PzIL1-doped PEDOT:PSS-based OLED device performances could be seen in Fig. 8. The device called 0.1 PzIL1, (0.1 ml PzIL1 was mixed in 1.0 ml PEDOT:PSS) exhibited maximum luminance 4185 cd.m^{-2} (Fig. 8a), maximum current efficiency 0.49 cd/A (Fig. 8b), the lowest turn-on voltage 1.86 V. (Here, turn-on voltage is a voltage value at 1 cd/m^2). In Fig. 8c, current density–voltage graphs showed that the current density values were higher than the reference device (without PzILs) values, except the device 2.0 PzIL1 (2.0 ml PzIL1 was mixed in 1.0 ml PEDOT:PSS); however, this device had poor performances, it could not be compared with the others. Therefore, current efficiency values were lower than the reference. The side-chain length of PzIL1 was shorter than PzIL2-4. When L_{max} values of PzIL1 with a five-membered spiro ring and PzIL3 with the same terminal methyl group end were compared, PzIL1 with a shorter side alkyl chain length showed a higher L_{max} (Table 3). EQE was 0.24% for 0.1 PzIL1. The device PzIL1 characteristics were enhanced upon decreasing ratio of ILs in PEDOT:PSS as summarized in Table 3. This enhancement was nearly valid for all PzIL1-4-based devices due to increasing ionic nature of PEDOT:PSS. This might affect the conductivity and charge carrier properties of HIL; therefore, it may cause changes in the physical properties of the films. The normalized EL spectra of the fabricated PzIL1 OLEDs were shown in Fig. 8d. EL spectrum exhibited peak at ~ 576 nm for the reference device (without PzILs), the behavior of the EL spectra did not change much, and Full Width Half Maximum (FWHM) was slightly shrinking. After

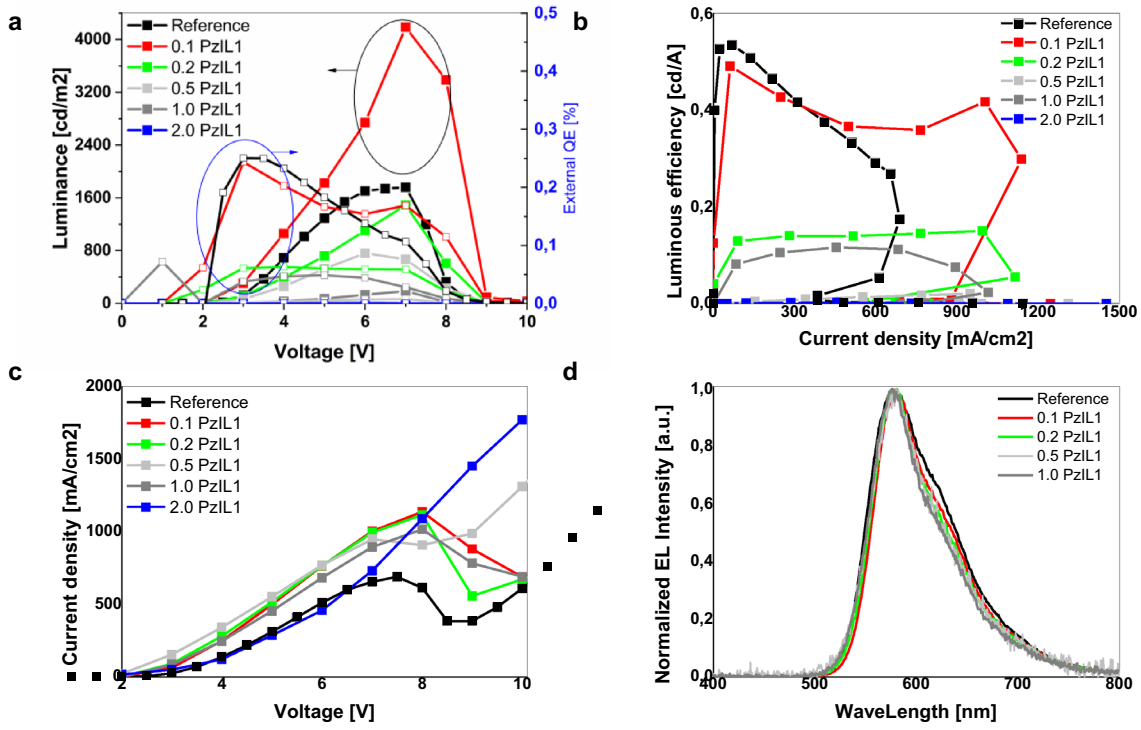


Fig. 8 **a** Luminance and EQE-voltage*, **b** luminous efficiency–current density, **c** current density–voltage and **d** normalized EL intensity characteristic of OLEDs fabricated with various ratios of PzIL1.*Solid square and open square belonged to luminance and EQE, respectively

Table 3 Summary of OLED device performances depending on different doped PzIL1-4 of the PEDOT:PSS

Device name	Concentration	V_{on}(V)	L_{max}(cd/m^2)	η_{max} (cd/A)	EQE (%)	Peak wavelength (nm)
Reference	–	2.00	1759	0.535	0.250	576
PzIL1	0.1	1.86	4190	0.491	0.244	580
	0.2	2.00	1490	0.150	0.063	580
	0.5	2.00	189.8	0.020	0.008	580
	1.0	2.18	762.0	0.116	0.044	577
	2.0	4.09	10.82	0.002	0.001	–
PzIL3	0.1	2.04	2348	0.496	0.235	585
	0.2	2.33	1709	0.966	0.479	581
	0.5	2.33	1564	0.588	0.274	587
	1.0	2.33	1175	0.501	0.233	582
	2.0	3.05	182.5	0.046	0.017	576
PzIL4	0.1	2.01	2801	0.577	0.969	572
	0.2	2.01	3180	0.598	0.279	578
	0.5	2.22	2012	0.573	0.276	583
	1.0	2.43	1426	0.450	0.206	582
	2.0	3.03	184.6	0.154	0.072	576
PzIL2	0.1	2.05	3082	0.707	0.328	581
	0.2	2.24	1492	0.521	0.239	573
	0.5	2.24	2120	0.554	0.255	577
	1.0	2.05	689.1	0.236	0.103	570
	2.0	2.64	181.5	0.040	0.019	578

all, it was compatible with the MEHPPV EL characteristics. The EL spectrum of the device 2.0 PzIL1 could not be presented here due to its poor performances.

In Fig. 9, the performance of the PzIL3-doped devices with different ratios could be seen. PzIL3 possessed five-membered spiro ring and a terminal methyl group. The 0.2 PzIL3 device performance exhibited second high maximum luminance 1709 cd m^{-2} (Fig. 9a). It had maximum current efficiency 0.96 cd/A due to low current density and EQE 0.48% (Fig. 9b), with turn-on voltage 2.33 V. These values were also the best EQE compared to all devices fabricated in this study. The device 0.1 PzIL3 had the maximum luminous with 2348 cd m^{-2}. In Fig. 9c, current density–voltage graphs showed that the current density values were close to the reference values (without PzILs), except for 0.2–2.0 ml ratios. The current density was low when compared to others, which means that the internal resistivity of the device was higher than the others.

The normalized EL spectra of the fabricated PzIL3 OLEDs were shown in Fig. 9d. EL spectrum exhibited peak at ~ 581 nm for the best performance device, the behaviors of the EL spectra were compatible with the MEHPPV EL characteristics.

In Fig. 10, PzIL4 device performances could be seen. The device performance named 0.2 PzIL4 exhibited 3180 cd m^{-2} luminance (Fig. 10a). It had current efficiency 0.598 cd/A (Fig. 10b), with turn-on voltage 2.01 V due to low current density. Comparing the L_{max} values of PzIL3 and PzIL4 with five-membered spiro ring and the same side alkyl chain length, PzIL4 with a longer terminal ethyl group (CH_2CH_3) showed a higher L_{max} value (Table 3). The principle of the spiro structure on affecting charge mobility and charge injection capability of the HILs, and the related OLED device performance was not taking part in the literature. As it is well known, isotropic properties play an important role in the efficient charge transfer in single spiro ring-based molecules, such as charge transfer in different directions [51,52]. Compared to single spiro core-based hole materials, dispiro-based materials with larger π conjugated system in the core unit can support molecules of higher stiffness and crystallinity which is good for improving hole mobility in the film. The device with 0.1 PzIL4 had the maximum EQE with 0.369%. In Fig. 10c, current density–voltage graphs showed that the current density values were close to the reference values, except for 2.0 ml ratios. The normalized EL spectra of the fabricated PzIL4 OLEDs were shown in Fig. 10d. EL spectrum exhibited peak at ~ 581 nm for the best performance device, the behavior of the EL spectra was also compatible with the MEHPPV EL characteristics.

In Fig. 11, PzIL2 device performances could be seen. The PzIL2 had six-membered spiro ring. Comparing the Lmax values of PzIL2 and PzIL3 with the same terminal methyl group and the same side alkyl chain length, PzIL2 with a six-membered spiro ring showed a higher Lmax value (Table 3). The larger π-conjugation length of the spiro ring was expected to present better π–π stacking in the HILs, leading to higher carrier mobility [53]. The mobility of

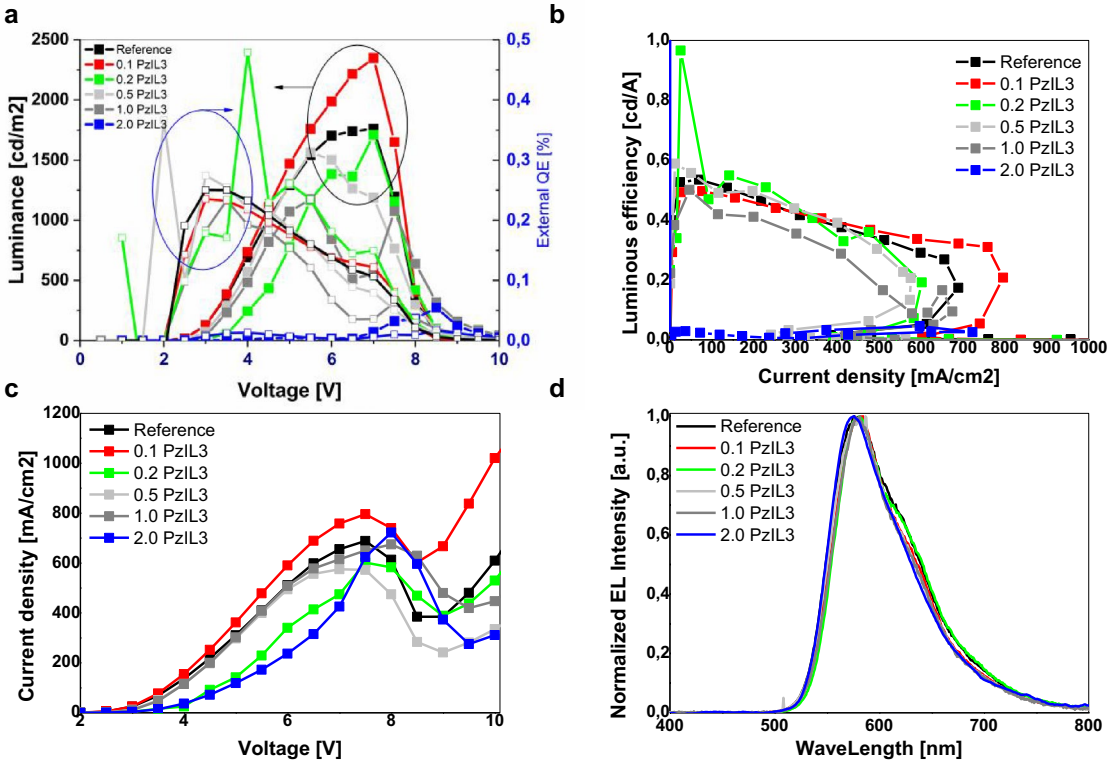


Fig. 9 **a** Luminance and EQE-voltage*, **b** luminous efficiency–current density, **c** current density–voltage and **d** normalized EL intensity characteristic of OLEDs fabricated with various ratios of PzIL3. *Solid square and open square belonged to luminance and EQE, respectively

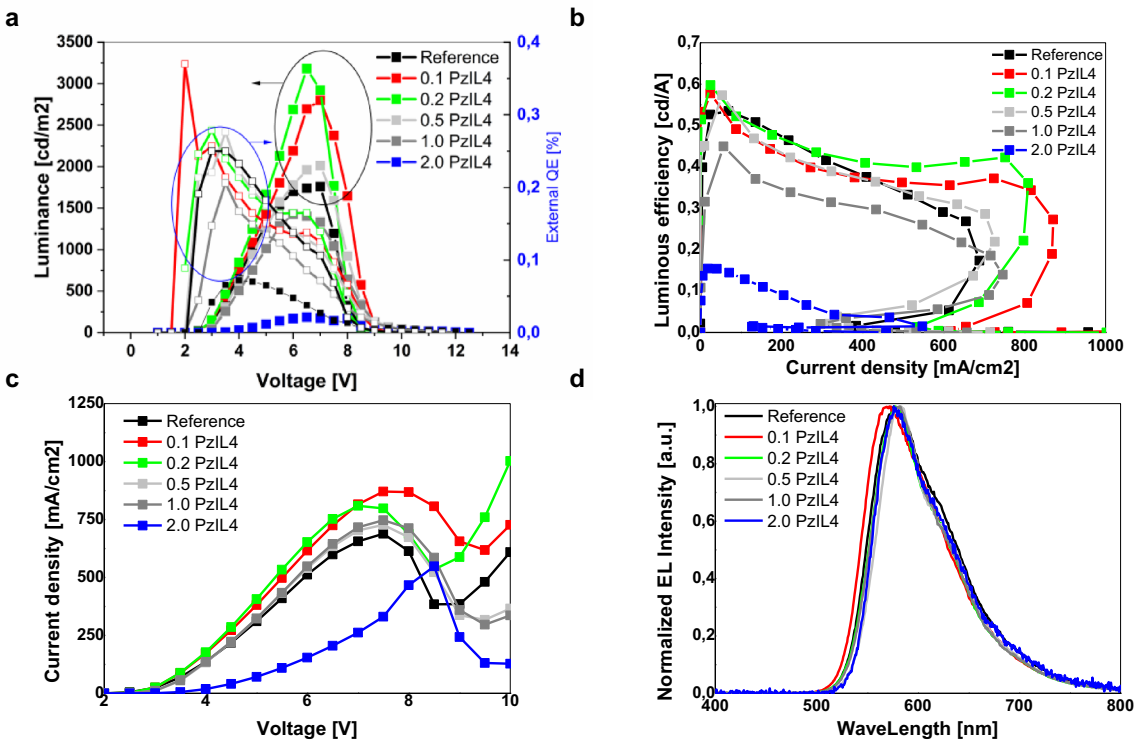


Fig. 10 **a** Luminance and EQE-voltage*, **b** luminous efficiency–current density, **c** current density–voltage and **d** normalized EL intensity characteristic of OLEDs fabricated with various ratios of PzIL4. *Solid square and open square belonged to luminance and EQE, respectively

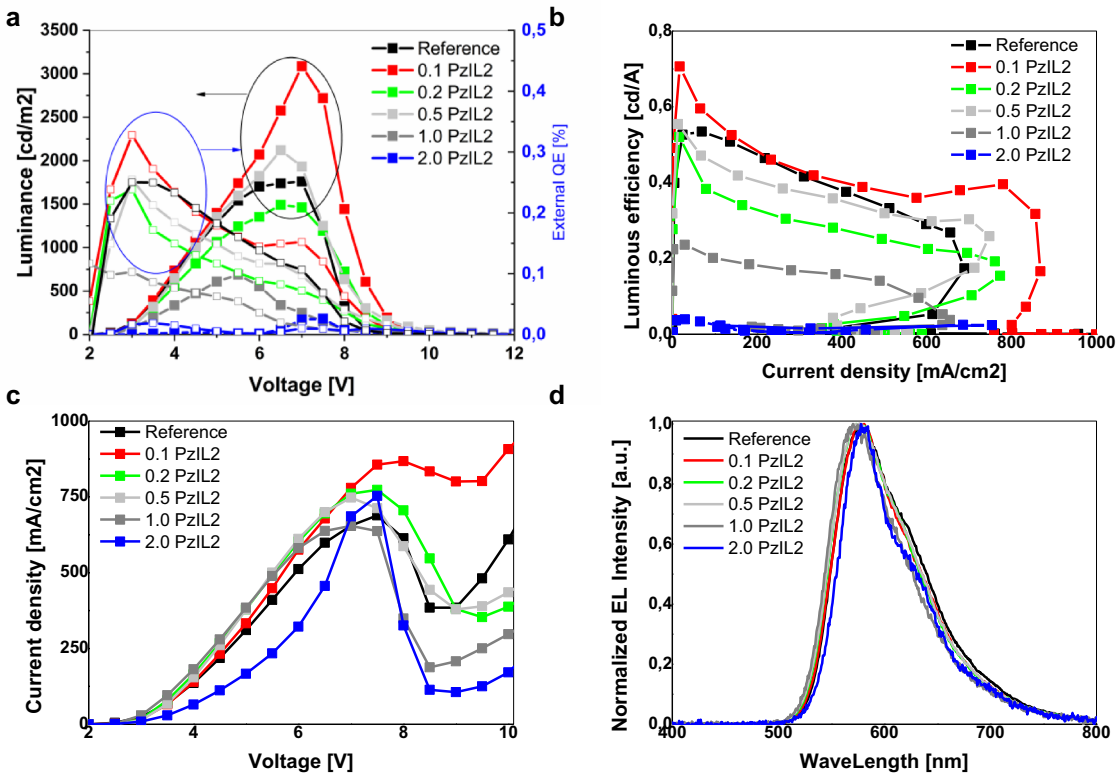


Fig. 11 **a** Luminance and EQE-voltage*, **b** luminous efficiency–current density, **c** current density–voltage, **d** normalized EL intensity characteristic of OLEDs fabricated with various ratios of PzIL2. *Solid square and open square belonged to luminance and EQE, respectively

PzIL2 was 1.78 cm^2/Vs. The device performance named 0.1 PzIL2, exhibited 3086 cd m^{-2} luminance with turn-on voltage 2.05 V (Fig. 11a). It had current efficiency 0.707 cd/A (Fig. 11b), due to low current density. The device named 0.1 PzIL2 had the maximum EQE with 0.328%. In Fig. 11c, current density–voltage graphs showed that the current density values were close to the reference values (without PzILs), except for 2.0 ml ratio. The normalized EL spectra of the fabricated PzIL2 OLEDs were shown in Fig. 11d. EL spectrum exhibited a peak at ~ 581 nm for the best performance device, the behavior of the EL spectra was compatible with the MEHPPV EL characteristics as the other PzILs.

In Fig. 12a, transparent PzIL1-4 thin films were prepared by spin-coating technique at 3000 rpm, there were no luminosity from the films. In Fig. 12b, optical microscope images of the PzIL1-4 thin films are with 500 × magnification (50 × from lens*10 × from camera). The films were homogenous. These images were proofs of the low roughness values for the AFM images.

In Fig. 13, AFM images of the PEDOT:PSS: PzIL1-4 blend thin films could be seen. The roughness values were < 2.0 nm and films had minor aggregation

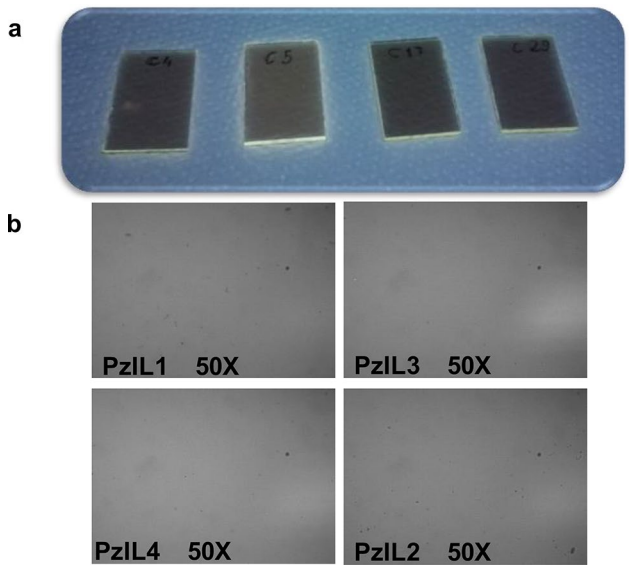


Fig. 12 **a** Thin films under Ultraviolet light**, b** thin-film images with Optical Microscope of PzIL1-4

characteristics, but this aggregation did not effect HIL thin-film morphology in the OLEDs devices.

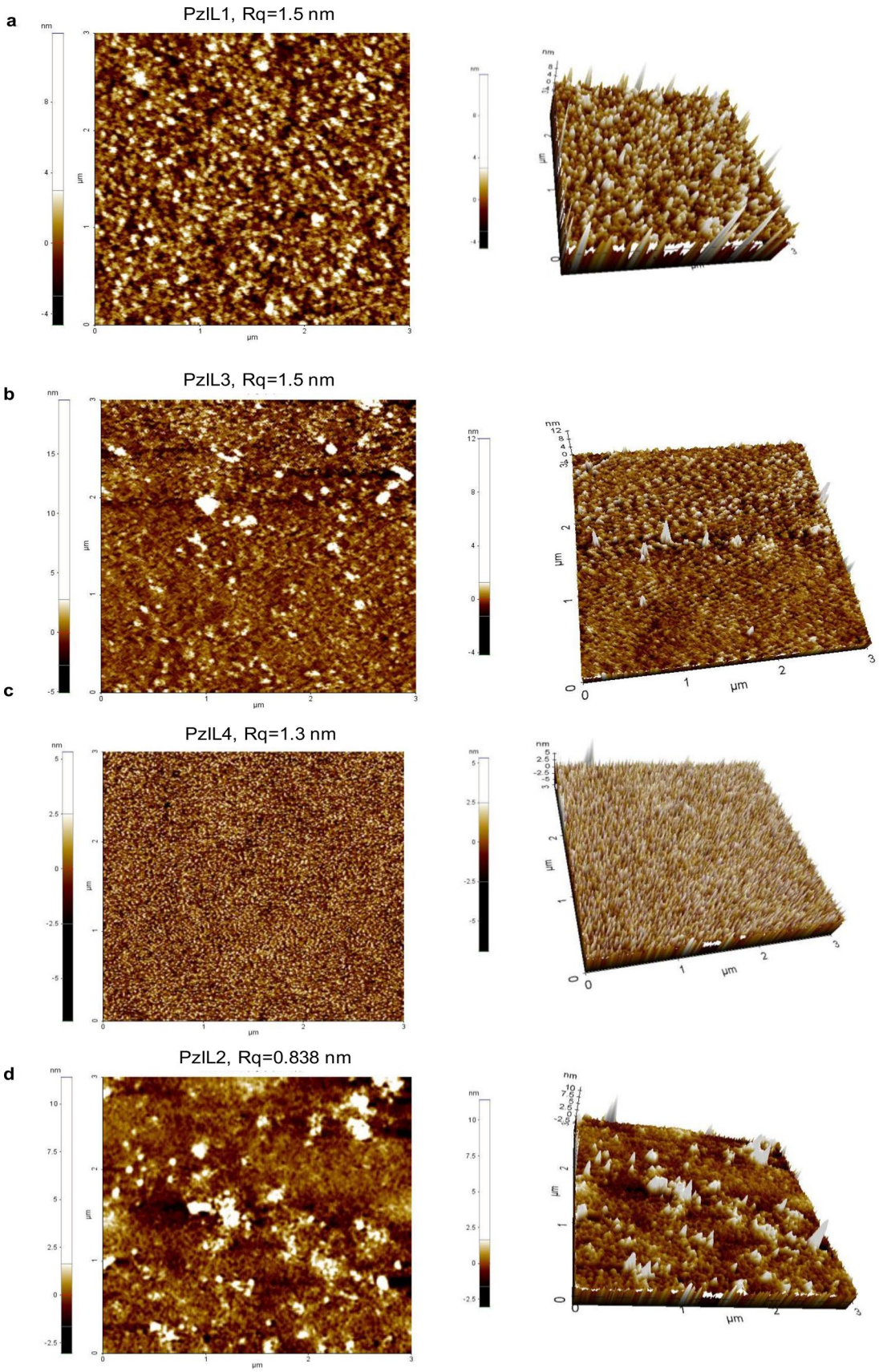


Fig. 13 AFM images of thin films of **a** PzIL1, **b** PzIL3, **c** PzIL4 and **d** PzIL2

3 Conclusion

The introduction of new ILs is producing creating a new application area. The important numbers of IL have been already synthesized as in this study, therefore, the potential of innovative ILs that will be developed according to the OLED performance requirements could be high for opto-electronic industry.

In conclusion, we have demonstrated efficient PzILs solution-processed OLEDs. Theoretical studies with DFT analysis were done to understand the physical basis behind it. Usage of PzILs led to an enhanced turn-on voltage, luminance and current efficiency that improved charge carrier injection into the light-emitting layer.

The L_{max} value of PzIL 1-4 with the same anion was influenced by the size of the spiro ring of the phosphazenium cation, the terminal alkyl group and the side-chain lengths bonded to the phosphorus atoms. As a result, shorter side-chain length, longer terminal alkyl group and bigger spiro ring yield higher L_{max} value. Therefore, the recombination possibility of charge carriers can be improved to make an efficient OLEDs. The device with PzIL1 exhibited the best performance with luminance 4185 cd/m^2 and mobility 1.93 cm^2/V.s compared to other devices with and without PzILs.

Acknowledgements The authors thank the Scientific and Technical Research Council of Turkey (TUBITAK, Grant KBAG-114Z740; COST Action CM 1206) for financial support.

Compliance with ethical standards

Conflicts of interests The authors declare that they have no known competing financial interests or personal relationships that could have appeared to influence the work reported in this paper.

References

1. Y.-S. Tyan, J. Photonics. Energy. **1**, 011009 (2011)
2. S. Reineke, F. Lindner, G. Schwartz, N. Seidler, K. Walzer, B. Lüssem, K. Leo, Nature **459**, 234 (2009)
3. T.-H. Han, Y. Lee, M.-R. Choi, S.-H. Woo, S.-H. Bae, B.H. Hong, J.-H. Ahn, T.-W. Lee, Nat. Photonics. **6**, 105 (2012)
4. Q. Zhang, B. Li, S. Huang, H. Nomura, H. Tanaka, C. Adachi, Nat. Photonics. **8**, 326 (2014)
5. Y.-H. Duan, Y. Duan, X. Wang, D. Yang, Y.-Q. Yang, P. Chen, F.-B. Sun, K.-W. Xue, Y. Zhao, Appl. Surf. Sci. **351**, 445 (2015)
6. P. Ho, J. Kim, J. Burroughes, H. Becker, S. Li, Nature **404**, 481 (2000)
7. H. Youn, M. Yang, Appl. Phys. Lett. **97**, 266 (2010)
8. K.S. Yook, J.Y. Lee, Adv. Mater. **26**, 4218 (2014)
9. P.L. Burn, S.C. Lo, I.D. Samuel, Adv. Mater. **19**, 1675 (2007)
10. N. Aizawa, Y.-J. Pu, M. Watanabe, T. Chiba, K. Ideta, N. Toyota, M. Igarashi, Y. Suzuri, H. Sasabe, J. Kido, Nat. Commun. **5**, 5756 (2014)
11. H. Ishii, K. Sugiyama, E. Ito, K. Seki, Adv. Mater. **11**, 605 (1999)
12. T. Chiba, Y.-J. Pu, J. Kido, J. Mater. Chem. C. **3**, 11567 (2015)
13. T. Nguyen, P. Le Rendu, P. Long, S. De Vos, Surf. Coat. Technol. **180**, 646 (2004)
14. C. Zhong, C. Duan, F. Huang, H. Wu, Y. Cao, Chem. Mater. **23**, 326 (2011)
15. T. Aernouts, P. Vanlaeke, W. Geens, J. Poortmans, P. Heremans, S. Borghs, R. Mertens, R. Andriessen, L. Leenders, Thin Solid Films **451**, 22 (2004)
16. M. Jaymand, Prog. Polym. Sci. **38**, 1287 (2013)
17. J. Jang, J. Ha, K. Kim, Thin Solid Films **516**, 3152 (2008)
18. T. Kugler, W. Salaneck, H. Rost, A. Holmes, Chem. Phys. Lett. **310**, 391 (1999)
19. L.A. Pettersson, S. Ghosh, O. Inganäs, Org. Electron. **3**, 143 (2002)
20. F. Zhang, M. Johansson, M.R. Andersson, J.C. Hummelen, O. Inganäs, Adv. Mater. **14**, 662 (2002)
21. J. Kim, J. Jung, D. Lee, J. Joo, Synth. Met. **126**, 311 (2002)
22. C. Lee, J. Kim, D. Lee, Y. Koo, J. Joo, S. Han, Y. Beag, S. Koh, Synth. Met. **135**, 13 (2003)
23. J. Luo, D. Billep, T. Waechtler, T. Otto, M. Toader, O. Gordan, E. Sheremet, J. Martin, M. Hietschold, D.R. Zahn, J. Mater. Chem. A. **1**, 7576 (2013)
24. H. Akbaş, A. Karadağ, A. Destegül, Ç. Çakırlar, Y. Yerli, K.C. Tekin, U. Malayoğlu, Z. Kılıç, New. J. Chem. **43**, 2098 (2019)
25. A. Destegül, H. Akbaş, A. Karadağ, B. Canımkurbey, Y. Yerli, K.C. Tekin, U. Malayoğlu, Z. Kılıç, Ionics **25**, 3211 (2019)
26. J.S. Wilkes, M.J. Zaworotko, J. Chem. Soc. Chem. Commun. **13**, 965–967 (1992)
27. J.S. Wilkes, Green. Chem. **4**, 73 (2002)
28. R.D. Rogers, K.R. Seddon, Science **302**, 792 (2003)
29. G. Pıhtılı, E. Çil, K. Koran, F. Özen, M. Arslan, G. Torğut, A. O. Görgülü **79**, 213–220 (2014)
30. H. Ozay, O. Ozay, Coll. Surf. A. **450**, 99 (2014)
31. Q. He, H. Dai, X. Tan, X. Cheng, F. Liu, C. Tschierske, J. Mater. Chem. C. **1**, 7148 (2013)
32. X. Wang, A.Y.X. Tan, C.M. Cho, Q. Ye, C. He, R. Ji, H.Q. Xie, J.W.H. Tsai, J. Xu, Tribol. Int. **90**, 257 (2015)
33. K. Inoue, T. Yamauchi, T. Itoh, E. Ihara, J. Inorg. Organomet. Polym. Mater. **17**, 367 (2007)
34. S. Ahn, H.-S. Kim, S. Yang, J.Y. Do, B.H. Kim, K. Kim, J. Electroceram. **23**, 289 (2009)
35. T. Nishimoto, T. Yasuda, S.Y. Lee, R. Kondo, C. Adachi, Mater. Horizons. **1**, 264 (2014)
36. P. Schrögel, M. Hoping, W. Kowalsky, A. Hunze, G. Wagenblast, C. Lennartz, P. Strohriegl, Chem. Mater. **23**, 4947 (2011)
37. C. Pozo-Gonzalo, R. Marcilla, M. Salsamendi, D. Mecerreyes, J.A. Pomposo, J. Rodríguez, H.J. Bolink, J. Polym. Sci. Part A. Polym. Chem. **46**, 3150 (2008)
38. T.Y. Kim, T.H. Lee, J.E. Kim, R.M. Kasi, C.S. Sung, K.S. Suh, J. Polym. Sci. Part A. Polym. Chem. **46**, 6872 (2008)
39. T. Kim, M. Suh, S.J. Kwon, T.H. Lee, J.E. Kim, Y.J. Lee, J.H. Kim, M. Hong, K.S. Suh, Macromol. Rapid Commun. **30**, 1477 (2009)
40. S.J. Kwon, T.Y. Kim, B.S. Lee, T.H. Lee, J.E. Kim, K.S. Suh, Synth. Met. **160**, 1092 (2010)
41. H. Brine, J.F. Sánchez-Royo, H.J. Bolink, Org. Electron. **14**, 164 (2013)
42. S. Ohisa, Y.-J. Pu, J. Kido, J. Mater. Chem. C. **4**, 6713 (2016)
43. P. S. Pro, Wavefunction Inc., 18401 Von Karman Avenue, Suite 370, Irvine, CA 92612, USA.
44. S. Forsyth, J. Golding, D.R. Macfarlane, M. Forsyth, Electrochim. Acta **46**, 1753 (2001)
45. J. L. Gázquez, Chem. Hardness. Springer. pp 27–43 (1993)
46. P.B. Ishai, M.S. Talary, A. Caduff, E. Levy, Y. Feldman, Meas. Sci. Technol. **24**, 102001 (2013)
47. J.Y. Fu, Phil. Mag. **94**, 1788 (2014)

48. S. Ono, S. Seki, R. Hirahara, Y. Tominari, J. Takeya, Appl. Phys. Lett. **92**, 93 (2008)
49. Y.D. Park, D.H. Kim, Y. Jang, J.H. Cho, M. Hwang, H.S. Lee, J.A. Lim, K. Cho, Org. Electron. **7**, 514 (2006)
50. S.P. Mucur, E. Tekin, Turk. J. Phys. **42**, 1 (2018)
51. J. Zhang, Y. Hua, B. Xu, L. Yang, P. Liu, M.B. Johansson, N. Vlachopoulos, L. Kloo, G. Boschloo, E.M. Johansson, Adv. Energy. Mater. **6**, 1601062 (2016)
52. D. Beaudoin, J.-N. Blair-Pereira, S. Langis-Barsetti, T. Maris, J.D. Wuest, J. Org. Chem. **82**, 8536 (2017)
53. B. Xu, J. Zhang, Y. Hua, P. Liu, L. Wang, C. Ruan, Y. Li, G. Boschloo, E.M. Johansson, L. Kloo, Chem **2**, 676 (2017)

Publisher's Note Springer Nature remains neutral with regard to jurisdictional claims in published maps and institutional affiliations.